Quasiballistic heat transfer studied using the frequency-dependent Boltzmann transport equation

A. J. Minnich, G. Chen, S. Mansoor, and B. S. Yilbas

Phys. Rev. B **84**, 235207 — Published 15 December 2011

DOI: 10.1103/PhysRevB.84.235207

Quasiballistic heat transfer studied using the frequency-dependent Boltzmann transport equation

A. J. Minnich,[1] G. Chen,[2,*] S. Mansoor,[3] and B. S. Yilbas[3]

[1]*Department of Mechanical and Civil Engineering*
California Institute of Technology
Pasadena, CA 91106
[2]*Department of Mechanical Engineering*
Massachusetts Institute of Technology
Cambridge, MA 02139
[3]*Department of Mechanical Engineering*
King Fahd University of Petroleum and Minerals
Dhahran, Saudi Arabia

Quasiballistic heat transfer occurs when there is a temperature gradient over length scales comparable to phonon MFPs. This regime has been of interest recently because observing quasiballistic transport can lead to useful information about phonon mean free paths (MFPs), knowledge of which is essential for engineering nanoscale thermal effects. Here, we use the Boltzmann transport equation (BTE) to understand how observations of quasiballistic transport can yield information about MFPs. We solve the transient, one-dimensional, frequency-dependent BTE for a double layer structure of a metal film on a substrate, the same geometry that is used in transient thermoreflectance experiments, using a frequency-dependent interface condition. Our results indicate that phonons with MFPs longer than the thermal penetration depth do not contribute to the measured thermal conductivity, providing a means to probe the MFP distribution. We discuss discrepancies between our simulation and experimental observations which offer opportunities for future investigation.

PACS numbers:

I. INTRODUCTION

Classical size effects in heat transfer, where the characteristic length scales of a system are comparable to phonon mean free paths (MFPs), have long been of interest.[1–4] The ability to create nanostructured materials has led to many observations of modified thermal properties in nanoscale systems.[4,5] Another type of size effect can occur if there is a temperature gradient over length scales comparable to phonon MFPs.[6] In this case, local thermal equilibrium does not exist and the transport is quasiballistic. Transient ballistic transport has been studied experimentally using heat pulse techniques and x-ray diffraction techniques.[7,8] A nonlocal theory of heat transport was proposed as a modification of diffusion theory[9]. It was also predicted that the heat conduction from a nanoparticle is significantly reduced from the Fourier law prediction[10].

Recently, several workers have used observations of quasiballistic heat transfer to infer information about phonon mean free paths (MFPs).[11–14] In particular, Koh and Cahill reported that varying the thermal penetration depth by changing the modulation frequency in a transient thermoreflectance (TTR) experiment can yield information about MFPs.[12] They explained their experimental observations using a simplified model based on the phonon Boltzmann transport equation (BTE).[15]

The full phonon BTE is often used to calculate heat transfer in the quasiballistic regime. The BTE has been solved using various numerical techniques in recent years, including with discrete ordinates[2,16], Monte Carlo techniques[17–19], and a finite volume approach.[20] However, many studies used frequency averaged properties. In a material such as Si, where phonon MFPs can vary by six orders of magnitude over the Brillouin zone,[21] this assumption is not realistic. While some studies did include frequency dependence,[2,16,18,20] several of these studies made other simplifying assumptions regarding the calculation of the equilibrium distribution function which are not self-consistent. A calculation of the phonon transport through a single material, including dispersion and polarization, has been reported,[20] but phonon transmission through an interface was not included.

Here, we numerically solve the transient, one-dimensional, frequency-dependent BTE, including polarization, both to examine how phonon MFPs can be extracted from measurements of quasiballistic heat transfer and to better understand Koh and Cahill's observations. We solve the equation for a double layer structure of a metal film on a substrate, the same geometry as that used in TTR, using the method of discrete ordinates. We use a frequency-dependent interface condition to account for differences in phonon dispersion between the two materials. Our results indicate that phonons with MFPs longer than the thermal penetration depth do not contribute to the measured thermal conductivity, providing a means to probe the MFP distribution. We discuss discrepancies between our simulation and experimental observations which offer opportunities for future investigation.

II. THEORY

The transient, one-dimensional, frequency-dependent phonon BTE is given by:[2]

$$\frac{\partial f_\omega}{\partial t} + \mu v_\omega \frac{\partial f_\omega}{\partial x} = -\frac{f_\omega - f_\omega^0}{\tau_\omega} \tag{1}$$

Here $f_\omega = \hbar\omega D(\omega) g(\omega)/4\pi$ is the desired distribution function, where $\hbar$ is Planck's constant divided by 2π, ω is the angular frequency, $D(\omega)$ is the phonon density of states, and $g(\omega)$ is the occupation function; f_ω^0 is the equilibrium distribution function, $\mu = \cos\theta$ is the cosine of the angle between the propagation direction and the x-axis, and τ_ω is the frequency dependent relaxation time. The equilibrium distribution f_ω^0 is given by

$$f_\omega^0(T) = \frac{\hbar\omega D(\omega) f_{BE}(T)}{4\pi} \tag{2}$$

where $f_{BE}(T) = (\exp(\hbar\omega/k_B T) - 1)^{-1}$ is the Bose-Einstein distribution function and T is the temperature of the distribution. The factors of 4π normalize the distribution by the solid angle. Other treatments of the BTE[2,16] have written the equation in terms of the intensity $I_\omega = f_\omega v_\omega$; however, for transient transport optical phonons must be included in the calculation but have essentially zero group velocity. To allow for the case of zero group velocity, we remove velocity from the definition of the distribution function.

For this study, we will take the materials to be an Al film on a Si substrate because these materials are commonly studied using TTR. The Al film requires additional examination. The total thermal conductivity of metals is often in the hundreds of W/mK range but electrons carry most of the heat. Here we only consider the thermal conduction due to the lattice to remove the thermal resistance from electron-phonon coupling.[22] The lattice thermal conductivity of the metal is not known with certainty; we use a value of $k_l \approx 30$ W/mK. Phonon relaxation times are also not well known in metals, and we take the relaxation time τ to be a constant so that $k = 1/3 \int C_\omega v_\omega^2 \tau d\omega$ gives the specified thermal conductivity.

We now discuss several important details of the calculation which must be treated properly to obtain a self-consistent solution.

A. Calculation of the equilibrium distribution

The equilibrium distribution f_ω^0 can be determined by integrating Eq. 1 with respect to frequency and angle and invoking conservation of energy.[2] The result is:

$$\int_0^{\omega_m} \int_{-1}^{1} \frac{f_\omega}{\tau_\omega} d\mu d\omega = \int_0^{\omega_m} \int_{-1}^{1} \frac{f_\omega^0}{\tau_\omega} d\mu d\omega \tag{3}$$

In the past, this equation has been satisfied by enforcing equality at each frequency, or $f_\omega^0 = 1/2 \int_{-1}^{1} f_\omega d\mu$.[2,16] However, it has been shown that this approximation will not give the correct solution to the BTE.[18] Therefore, it is necessary to determine the temperature T by integrating Eq. 3 over frequency and angle. To simplify the calculation, we approximate that the temperature difference throughout the domain is not too large. We can then linearize the equilibrium distribution:

$$f_\omega^0(T) = \frac{\hbar\omega D(\omega) f_{BE}(T)}{4\pi} \approx f_\omega^0(T_0) + \frac{C_\omega}{4\pi}\Delta T \tag{4}$$

where $\Delta T = T - T_0$. This gives a simpler equation for the temperature of the equilibrium distribution:

$$\Delta T = \frac{4\pi}{\int_0^{\omega_m} (C_\omega/\tau_\omega) d\omega} \int_0^{\omega_m} \int_{-1}^{1} \frac{f_\omega - f_\omega^0(T_0)}{\tau_\omega} d\mu d\omega \tag{5}$$

The equilibrium distribution then follows immediately from Eq. 4.

Solving for the equilibrium distribution in this manner significantly complicates the solution. Since all the frequencies are coupled, Eq. 5 must be solved at each spatial point. In silicon, phonon MFPs can vary from a few nanometers for zone-edge phonons to millimeters for long wavelength phonons, a six order of magnitude difference. To obtain a correct solution for short mean free path phonons, the numerical spatial grid must have a small step size. However,

to obtain a correct solution for the fast, long MFP phonons requires a large spatial domain. Since the solution must be known at every spatial point, these contradictory requirements imply a large domain with very fine spatial step size is required, making the solution computationally demanding. Multi-grid schemes, with a different spatial grid for each frequency, could be used, but to simplify numerical considerations we solve the distribution function for all frequencies on a single grid.

B. Role of optical phonons

Optical phonons are typically neglected in studies of phonon transport, as they contribute little to the thermal conductivity due to their near zero group velocity.[21] However, in transient heat transport, optical phonon modes with large specific heats act as a thermal capacitance and thus affect the transport, even if the modes do not actually transport any heat themselves.[20] We incorporate these phonons in Si (Al does not have optical phonons) simply as another mode with zero group velocity. We must also specify an optical phonon relaxation time; we use a value of 3 ps.[23] The solution is not sensitive to the precise value. The optical phonon specific heat is given by the Einstein model assuming three degenerate optical branches:[24]

$$C_{op} = 3Nk_B \left(\frac{\hbar\omega_{op}}{k_B T}\right)^2 \frac{\exp(\hbar\omega_{op}/k_B T)}{(\exp(\hbar\omega_{op}/k_B T)-1)^2} \tag{6}$$

where N is the number density of the material and ω_{op} is the optical phonon frequency, equal to 63 meV in Si.[25]

C. Interface condition

After the phonons travel through the metal film they reach the interface between the metal and substrate, where phonons are either transmitted or reflected. Presently, the details of these transmission or reflection processes are largely unknown. Molecular dynamics simulations have been used to study phonon transmission through coherent interfaces,[26,27] but it is not clear if these results are applicable to the imperfect interfaces encountered in experiment. Due to this lack of knowledge, we use a simplified frequency dependent interface condition. We assume elastic, diffuse scattering and neglect any type of mode conversion: phonons do not change frequency or polarization as they cross the interface, but are scattered equally in all directions. These assumptions allow the transmission and reflection processes for each phonon frequency to be treated independently. A diagram with the dispersions of Al and Si, along with the allowed scattering modes, is shown in Fig. 1.

To fully specify the phonon distribution at the interface, it is necessary to obtain the outgoing distributions from the interface, which are the backward-going phonons on side 1, $f^-_{\omega 1}$, and the forward-going phonons on side 2, $f^+_{\omega 2}$; as a function of the incoming distribution to the interface, which are the forward-going phonons on side 1, $f^+_{\omega 1}$, and the backward-going phonons on side 2, $f^-_{\omega 2}$. These outgoing distributions are obtained by enforcing that the heat fluxes from $f^-_{\omega 1}$ and $f^+_{\omega 2}$ are equal to the reflected and transmitted heat fluxes from $f^+_{\omega 1}$ and $f^-_{\omega 2}$. Because we assume elastic scattering and neglect mode conversion, the heat flux equality condition must be satisfied for each frequency and polarization. The conditions are:

$$q^+_{\omega 1} = \int_0^1 f^+_{\omega 1} v_{\omega 1} \mu d\mu \tag{7}$$

$$q^-_{\omega 2} = \int_{-1}^0 f^-_{\omega 2} v_{\omega 2} \mu d\mu \tag{8}$$

$$f^+_{\omega 2} v_{\omega 2} = 2\left(T_{12}(\omega) q^+_{\omega 1} - R_{21}(\omega) q^-_{\omega 2}\right) \tag{9}$$

$$f^-_{\omega 1} v_{\omega 1} = 2\left(-T_{21}(\omega) q^-_{\omega 2} + R_{12}(\omega) q^+_{\omega 1}\right) \tag{10}$$

Here $T_{12}(\omega)$ is the transmission coefficient from side 1 to 2, $R_{21}(\omega)$ is the reflection coefficient from side 2 back into side 2, and so on. These equations allow $f^-_{\omega 1}$ and $f^+_{\omega 2}$ to be determined and thus fully specify the distribution function at the interface.

We now examine the frequency dependent transmission and reflection coefficients. In order to be consistent with the two materials' dispersions and to satisfy the principle of detailed balance and the conservation of energy, there are several restrictions on the coefficients. Let us assume the frequency-dependent transmissivity from medium 1 to medium 2, $T_{12}(\omega)$, is specified. First, under the assumption of elastic scattering and the neglect of mode conversion, some high frequency phonons are unable to transmit from one material to the other due to a lack of a state. For Al

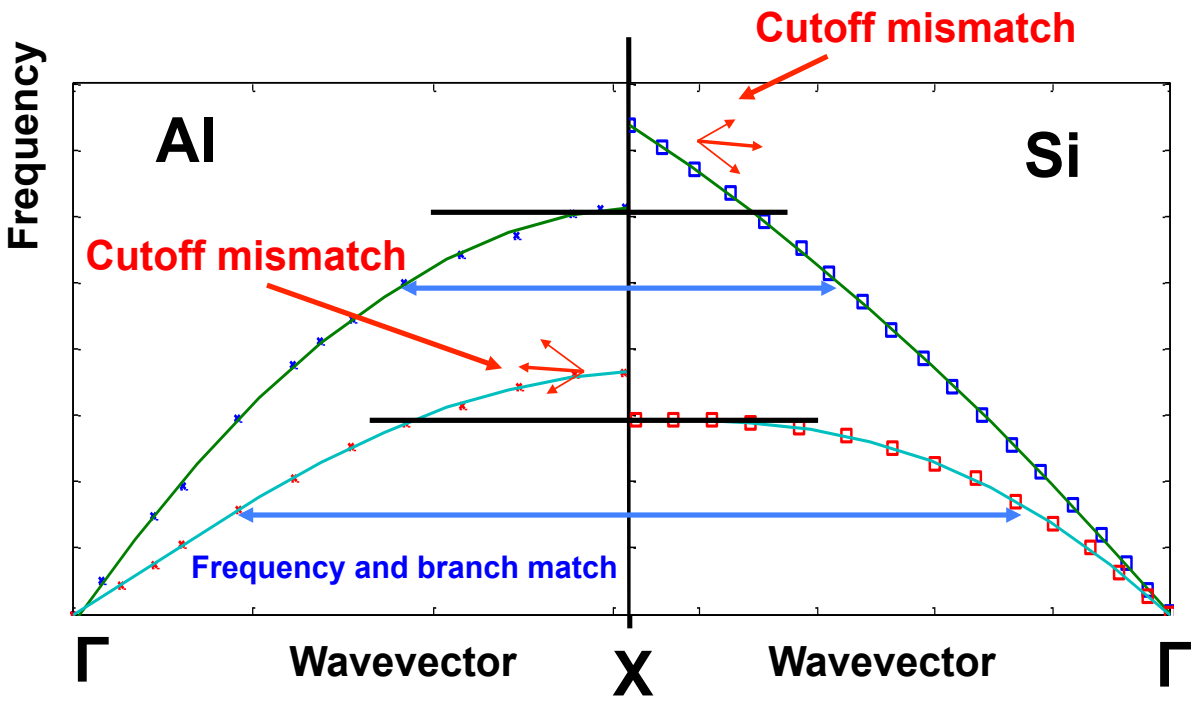

FIG. 1: Phonon dispersions of Al (left) and Si (right). Scattering is permitted between phonons of the same polarization and frequency. High frequency phonons lacking a corresponding state are diffusely backscattered, indicated by the cutoff mismatch in the figure.

and Si, this occurs for phonons in the Al transverse branch and the Si longitudinal branch. These phonons are not able to transmit and therefore have zero transmissivity; this is indicated by 'cutoff mismatch' in Fig. 1.

Next, the principle of detailed balance must be satisfied. This principle requires that when both materials are at an equilibrium temperature T, no net heat flux can transmit across the interface. This condition applies for every phonon mode on each side of the interface[28]:

$$T_{12}(\omega)f^0_{\omega 1}(T)v_{\omega 1} = T_{21}(\omega)f^0_{\omega 2}(T)v_{\omega 2} \tag{11}$$

Thus, even if $T_{12}(\omega)$ is frequency independent, $T_{21}(\omega)$ will in general be frequency dependent. Because we have assumed diffuse scattering, none of the transmission or reflection coefficients are angle-dependent and no further restriction is necessary.

Note that because $f^0_\omega(T)$ depends nonlinearly on T, temperature cannot be extracted from Eq. 11, meaning that the relationship between $T_{12}(\omega)$ and $T_{21}(\omega)$ required to satisfy detailed balance will change depending on the phonon temperature. However, due to the small deviations from the equilibrium temperature T_0 considered here, to excellent approximation detailed balance can be satisfied for all the phonons by evaluating Eq. 11 at T_0.

Finally, conservation of energy is ensured by enforcing an equality of the heat fluxes on each side of the interface,[24] giving:

$$R_{12}(\omega) = 1 - T_{12}(\omega) \tag{12}$$
$$R_{21}(\omega) = 1 - T_{21}(\omega) \tag{13}$$

All of these conditions must be satisfied at every frequency and polarization. Using the above relations, once $T_{12}(\omega)$ is specified all of the other coefficients can be obtained.

The transmissivity $T_{12}(\omega)$ can be related to the interface conductance G by calculating the heat flux and equivalent equilibrium temperature on each side of the interface.[3] The interface conductance is defined as

$$G = q/\Delta T \tag{14}$$
$$q = \int_0^{\omega_m}\int_{-1}^{1} f_1 v_{\omega 1}\mu d\mu d\omega \tag{15}$$

where q is the heat flux at the interface and ΔT the temperature difference across the interface. The heat flux depends on the transmissivity, and therefore will be different from the results derived previously[3] due to the frequency dependence of the transmissivity.

The heat flux is straightforward to calculate from the distribution function f using Eq. 15, but defining the temperature difference ΔT is more subtle. Assuming that $f^+_{\omega 1}$ and $f^-_{\omega 2}$ have some emitted phonon temperature T_{e1} and T_{e2}, respectively, $f^+_{\omega 2}$ and $f^-_{\omega 1}$ will be composed of reflected and transmitted phonons at these different temperatures and will be strongly out of equilibrium.[3] It has been shown that the appropriate quantity to use is the equivalent equilibrium temperature, which represents the temperature of the distribution that a non-equilibrium phonon distribution would reach if it were to relax adiabatically to equilibrium.[3] Thus, even though the forward and backward going phonons are strongly out of equilibrium, using the equivalent equilibrium temperature allows the results to be compared to the Fourier's law result which assumes local thermal equilibrium.

Using Eq. 14, the heat flux q from Eq. 15, and the equivalent equilibrium temperature,[3] the modified relation between the interface conductance and transmissivity can be shown to be:

$$\left\langle T_{12}(\omega) f^0_{\omega 1} v_{\omega 1} \right\rangle = \frac{2}{\langle Cv \rangle_1^{-1} + \langle Cv \rangle_2^{-1} + (2G)^{-1}} \tag{16}$$

where $\langle \cdot \rangle$ denotes integration over frequency. If the transmissivity is frequency independent then this formula reduces to the result derived previously.[3] It is important to remember that this formula assumes that the incoming distributions to the interface, $f^+_{\omega 1}$ and $f^-_{\omega 2}$, have a temperature. If these distributions are also out of equilibrium, then it is not possible to relate the interface conductance and transmissivity. In this case, with the transmissivity specified, the interface conductance will change with time until the two incoming distributions do have a temperature, at which point Eq. 16 will be valid and the interface conductance will become a constant. Due to the transient nature of the heat transport studied here, the two distributions never exactly achieve a thermal distribution, and so the thermal conductance can still change slowly with time.

D. Phonon dispersion and relaxation times

We now need to specify the dispersion and relaxation times for both the Al film and the Si substrate. We use the experimental dispersion in the [100] direction for both Al and Si and assume the crystals are isotropic.

We assume a constant relaxation time τ for all modes in Al; the value $\tau = 10$ ps is chosen to yield the desired lattice thermal conductivity $k \approx 30$ W/mK. For Si, we use relaxation times for phonon-phonon scattering extracted from molecular dynamics (MD) simulations[29] but with an empirical term $\exp(-\theta/T)$ to extend the relaxation times to lower temperatures.[30] While other forms of the relaxation times are available, we have verified that the difference between the various relaxation times is not sufficient to affect our analysis in the subsequent sections. We also add boundary scattering and impurity/isotope scattering, which are important at $T < 100$ K, and combine the relaxation times using Matthiessen's rule $\tau^{-1} = \sum_i \tau_i^{-1}$. The relaxation times (in seconds) are:

$$\tau_L^{-1} = 2 \times 10^{-19} \times \omega^2 T^{1.49} \exp(-\theta/T) \tag{17}$$

$$\tau_T^{-1} = 1.2 \times 10^{-19} \times \omega^2 T^{1.65} \exp(-\theta/T) \tag{18}$$

$$\tau_I^{-1} = 3 \times 10^{-45} \times \omega^4 \tag{19}$$

$$\tau_B^{-1} = 1.2 \times 10^6 \tag{20}$$

where L and T denote longitudinal and transverse, respectively. The thermal conductivity is calculated with the above relaxation times using the kinetic theory expression for the thermal conductivity:

$$k = \frac{1}{3} \sum_p \int_0^{\omega_m} C_\omega v_\omega^2 \tau_\omega d\omega \tag{21}$$

where the sum is over polarization p. The exact dispersion is used in this calculation. As in Holland's model the additive term accounting for normal scattering is neglected.[30]

E. Numerical details and boundary conditions

We solve the BTE numerically using a discrete ordinates method.[16] Both the angle and frequency are discretized using Gaussian quadrature to minimize the number of points required. The angle is discretized into $N_\mu = 40$ points.

The frequency discretization is more complicated because of the cutoff frequency mismatch for zone-edge phonons. Integrals involving the phonon dispersion are split into two integrals, one over the modes in common between Al and Si and another over the remaining modes, which in this case is the high frequency modes of the Al T branch and the Si L branch. These integrals are then separately discretized using Gaussian quadrature. An explicit first-order finite difference method is used to discretize the spatial and temporal derivatives.[16]

In addition to the interface conditions, one boundary condition is required for each angle $-1 < \mu < 1$. The distribution function must be specified for angles $0 < \mu < 1$ at $x = 0$, or the top of the metal film, and for angles $-1 < \mu < 0$ at $x = L$, or the bottom of the substrate. Here L is the length of the numerical domain, taken to be 3 μm for the simulations at 300 K. We choose the boundary condition at $x = 0$ to be diffuse reflection so that this surface is adiabatic. For the boundary condition at $x = L$, the type of boundary condition used ideally should not matter if the domain is sufficiently long. We use adiabatic or constant temperature boundary conditions and confirm that the solution to the BTE is the same in both cases. To verify convergence of the numerical solution, the number of spatial points, angle points, and frequency points were all increased; the solution is again unchanged.

The initial condition is an exponentially decaying phonon temperature distribution, with the $1/e$ depth of the temperature profile taken to be the light absorption depth in Al, approximately 7 nm for visible wavelengths.[31] The Al layer thickness is 100 nm.

The interface transmissivity $T_{12}(\omega)$ is calculated using Eq. 16 for a particular value of G specified at the beginning of the simulation. The rest of the transmission and reflection coefficients can then be calculated as described in section II C.

III. RESULTS

To verify the code is working properly, we first consider a test case. In this simulation, performed at T=300 K, the maximum relaxation time was truncated to 10 ps, putting the transport easily into the diffusive limit. In this case, the solution from the BTE should be very close to the Fourier law solution. Figure 2a shows good agreement between the surface temperature of the metal film versus time predicted by the BTE and by Fourier's law.

We can also calculate the interface conductance G and compare it to the value specified at the beginning of the simulation. The interface conductance is obtained from the solution to the BTE $f(t, x, \mu)$ using Eq. 14. The result is shown in Fig. 2b; the calculated result is close to the specified value of 1.1×10^8 W/m^{2}K.

This test case demonstrates that the calculation successfully reproduces the diffusive limit and is operating properly. We now perform the same simulation, only with the restriction on relaxation times removed; relaxation times are now given by the equations in Sec. II D and can be arbitrarily long. The same figures as before, lattice surface temperature versus time and interface conductance versus time, are shown in Figs. 2c and 2d, respectively.

This calculation gives a different result than the test case. Examining Fig. 2c, we see that at room temperature the solution from the BTE does not match that from Fourier's law, indicating ballistic effects are present. This result highlights the importance of including frequency dependence in the calculation. While the average phonon MFP is estimated to be around 40 nm in Si,[24] more detailed analyses show that MFPs vary by 5-6 orders of magnitude over the Brillouin zone.[29] In terms of the present one-dimensional simulation, these long MFP (and relaxation time) phonon modes do not scatter over the timescale of the simulation, resulting in the failure of Fourier's law. From Fig. 2c, we see that the surface temperature decay curve is shallower than the Fourier law prediction, indicating that the heat transfer in the quasiballistic case is smaller than in the diffusive case. This reduced heat flux, or, equivalently, ballistic thermal resistance, in quasiballistic transport has been demonstrated experimentally in sapphire[11], in semiconductor alloys,[12] and in silicon at cryogenic temperatures.[13] The fundamental cause of ballistic thermal resistance as follows. When applying Fourier's law to a domain, we assume that there is phonon scattering in the domain for the heat diffusion picture to be valid. When Fourier's law is applied to a domain where no scattering occurs, Fourier's law implies fictitious scattering events take place in the domain, even though the phonon mean free path corresponding to the bulk material's thermal conductivity is much longer than the domain and no scattering actually happens. If we instead use the domain length rather than the much longer MFP to calculate thermal conductivity, the effective thermal conductivity in the ballistic case will be much smaller than the true value, yielding a larger thermal resistance.[10]

Examining the interface conductance in Fig. 2d, we see an additional change. Instead of a constant interface conductance close to the value of 1.1×10^8 W/m^{2}K specified, the interface conductance changes with time. The reason for this was discussed in Sec. II C. To define an interface conductance, the incoming distributions at the interface must have a thermal distribution. Due to the long relaxation times of some phonons, local thermal equilibrium does not exist over the short timescales of this simulation, making it impossible to define a constant interface conductance.

The effect of ballistic thermal resistance is much more apparent at T$<$ 300 K, where phonon relaxation times can be longer than 1 μs. The length of the domain in this case is 15 μm to remove any possibility of finite domain effects. A typical result is shown in Fig. 3 at T=100 K; ballistic effects are clearly evident.

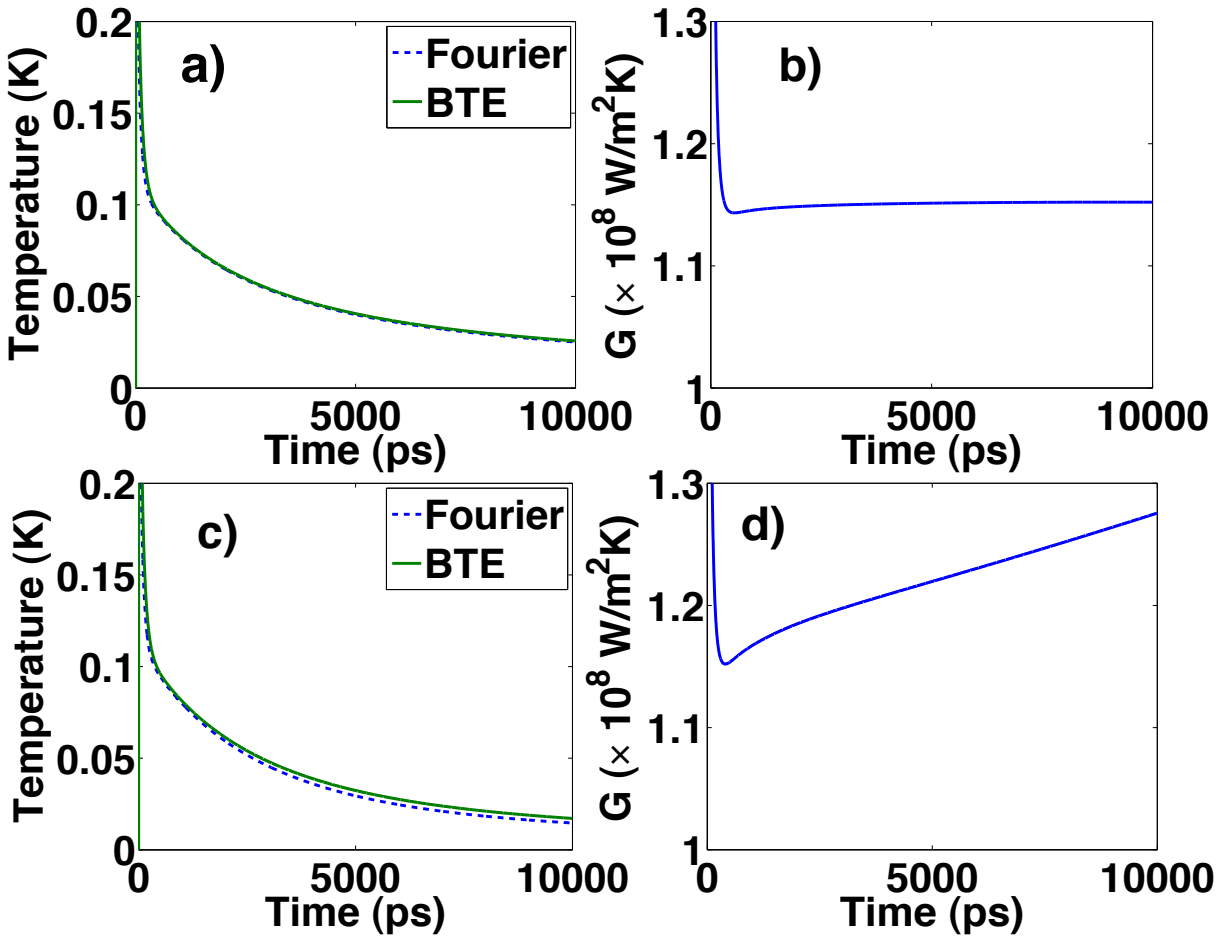

FIG. 2: (a) Lattice surface temperature (relative to a reference temperature of 300 K) versus time predicted by the BTE and the heat equation and (b) the interface conductance G calculated from the BTE with truncated relaxation times to 10 ps. (c) and (d) are the same figures except calculated with unmodified relaxation times which may be arbitrarily long. The surface temperature plot (a) with truncated relaxation time agrees almost exactly with the diffusive prediction, while case (c) shows a discrepancy due to quasiballistic effects. Similarly, the truncated relaxation time interface conductance (b) is essentially a constant close to the specified value of 1.1×10^8 W/m^{2}K, while the interface conductance in the unmodified case (d) changes with time.

IV. DISCUSSION

From the results presented, it is clear that qualitatively, the solution of the phonon BTE compared to the Fourier's law solution contains information about relaxation times. In particular, if the BTE solution is different than the Fourier's law solution, we can conclude that some phonon modes have relaxation time longer than the timescale of the simulation. The magnitude of the difference between the two solutions also gives some information about relaxation times: the longer the relaxation times, the larger will be the deviation and vice versa.

We would like to better understand which phonon modes are responsible for these discrepancies and determine how to extract information about relaxation times. As discussed in the previous section, quasiballistic transport results in a smaller heat flux than predicted by Fourier's law, corresponding to a smaller effective thermal conductivity. We can interpret the value of this effective thermal conductivity using an earlier work by Koh and Cahill[12]. Their work proposed that ballistic phonons, which have MFPs longer than the cross-plane thermal penetration depth, have effectively infinite ballistic thermal resistance and do not contribute to the thermal conductivity measured by the experiment. The effective thermal conductivity k_{eff} is due to short MFP phonons:

$$k_{eff} = \frac{1}{3}\int_0^{\Lambda_{co}} C_\omega v_\omega \Lambda_\omega d\Lambda_\omega \tag{22}$$

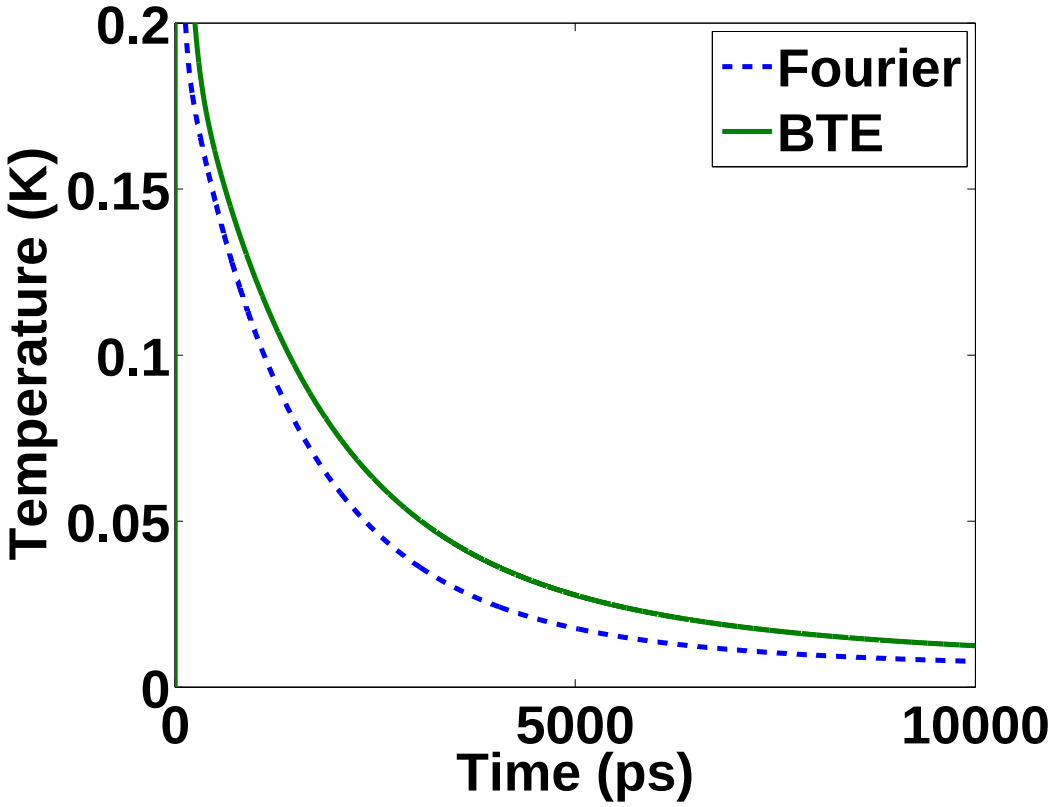

FIG. 3: Lattice surface temperature (relative to a reference temperature of 100 K) versus time predicted by the heat equation and BTE with full relaxation times at T = 100 K. Ballistic effects are more apparent at low temperatures where relaxation times are longer.

where Λ_{co} is the cutoff MFP, approximately equal to the thermal penetration depth. While Koh and Cahill's model is originally based on the penetration depth due to the accumulative effect of multiple pulses, to start we will consider the single pulse penetration depth.

To determine the effective thermal properties predicted from the BTE, we fit the single-pulse BTE solution with a Fourier's law solution using an effective thermal conductivity k_{eff} and interface conductance G_{eff}. The effective properties are obtained by manually adjusting the properties in the Fourier law model until the Fourier law solution matches the BTE solution. These properties will be smaller than the values specified in the BTE computation due to the ballistic thermal resistance. This fit is demonstrated in Fig. 4a for T=300 K. The BTE solution, in which $k = 140$ W/mK and G=1.1×10^8 W/m^{2}K were specified, matches a Fourier's law solution with different effective values of $k_{eff} = 100$ W/mK and $G_{eff} = 1.0 \times 10^8$ W/m^{2}K. Based on our manual fitting, we estimate the uncertainty in the fitted values is approximately 10%.

Because the net heat transfer from the metal film is smaller than the Fourier's law prediction, both the interface conductance and thermal conductivity are smaller than their specified values. Understanding how the interface conductance is affected by quasiballistic transport has not been considered previously and is an interesting topic for future study. This effect will not be further considered here, however.

Under Koh and Cahill's interpretation, the discrepancy between these two thermal conductivity values is due to long MFP phonon modes. For the single pulse case, $L_{pd} \approx 2 \times \sqrt{\pi \alpha t}$, where L_{pd} is the thermal penetration depth, $\alpha \approx 10^{-4}$ W/m^{2}K is the thermal diffusivity of silicon at T=300 K, and $t \approx 5$ ns is the approximate timescale of the experiment.[15] Using these values, we find that $L_{pd} \approx 2.5 \mu m$, suggesting that phonons with MFPs longer than a cutoff MFP of $\Lambda_{co} \approx 2.5$ μm do not contribute to the measured thermal conductivity. To determine if this value is reasonable, we use Eq. 22 to calculate the thermal conductivity with a cutoff MFP of 2.5 μm. The result is $k \approx 100$ W/mK, in good agreement with the value obtained from fitting the BTE solution.

The results of this fitting procedure for temperatures down to T=150 K are shown in Fig. 4b. At and below T = 100 K a satisfactory fit using Fourier's law is difficult to obtain for reasons that are presently unclear. However, above

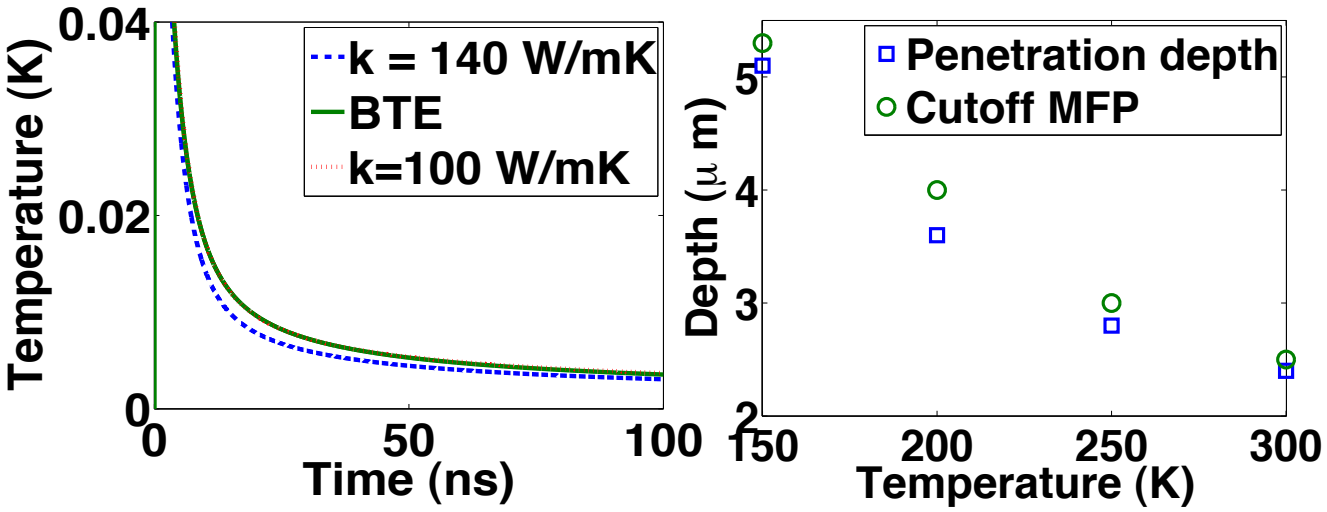

FIG. 4: (a) Surface temperature (relative to a reference temperature of 300 K) versus time predicted by the BTE (solid line), along with the solutions from Fourier's law for k=140 W/mK (dashed line) and k=100 W/mK (dotted line) at T = 300 K. The BTE solution almost exactly matches the curve with a reduced effective thermal conductivity of 100 W/mK. (b) Thermal penetration depths and cutoff MFPs required to obtain the effective thermal conductivity from the BTE solution. The two quantities agree well, supporting the idea that phonons with MFP longer than the penetration depth do not contribute to the measured thermal conductivity.

T=100 K, there is quite good agreement between the MFP cutoff values Λ_{co}, obtained from the frequency-dependent model of thermal conductivity, and the penetration depth L_{pd}. These results further support the hypothesis that phonons with $\Lambda_\omega > L_{pd}$ do not contribute to the measured thermal conductivity. Therefore, by performing an experiment in which the thermal penetration depth is shorter than some phonon MFPs, the MFP distribution can be probed by varying the penetration depth.

V. UNRESOLVED DISCREPANCIES

There are two discrepancies between our numerical analysis and experimental observations. First, while the single-pulse numerical simulations suggest that quasiballistic effects should be observable at room temperature in silicon at nanosecond timescales, experimentally the correct thermal conductivity is routinely measured using standard ultrafast techniques.[32] The reason for this discrepancy is presently unclear, but could be due to the accumulative effect of multiple pulses making the effective heat transfer timescale longer than that of the single pulse case.

Second, our simulation is presently not able to explain the modulation frequency dependence of thermal conductivity observed in Koh and Cahill's experiment. So far, we have only numerically solved for the single-pulse response of the BTE. As mentioned above, in a typical TTR experiment the observed response of a sample is actually due to multiple pulses.[32] Koh and Cahill's observation of modulation frequency-dependent thermal conductivity can only be interpreted using this multi-pulse response.

The multi-pulse response can be calculated from the single-pulse response using a procedure described in Ref. [32]. Briefly, the procedure involves adding later portions of the single-pulse response multiplied by a phase factor to the beginning of the single-pulse response:

$$Z(t) = \sum_{q=0}^{\infty} h(qT + t) e^{-i\omega_0 (qT+t)} \tag{23}$$

where $Z(t)$ is the multi-pulse response at time t, h is the single-pulse response, T is the time between laser pulses, and ω_0 is the modulation frequency. The modulation frequency affects the multi-pulse response by changing the phase factor multiplying the single-pulse response.

In the diffusive limit, the multi-pulse response and impulse response should both correspond to the same thermal conductivity value, regardless of the modulation frequency used. In order to measure a modulation-frequency depen-

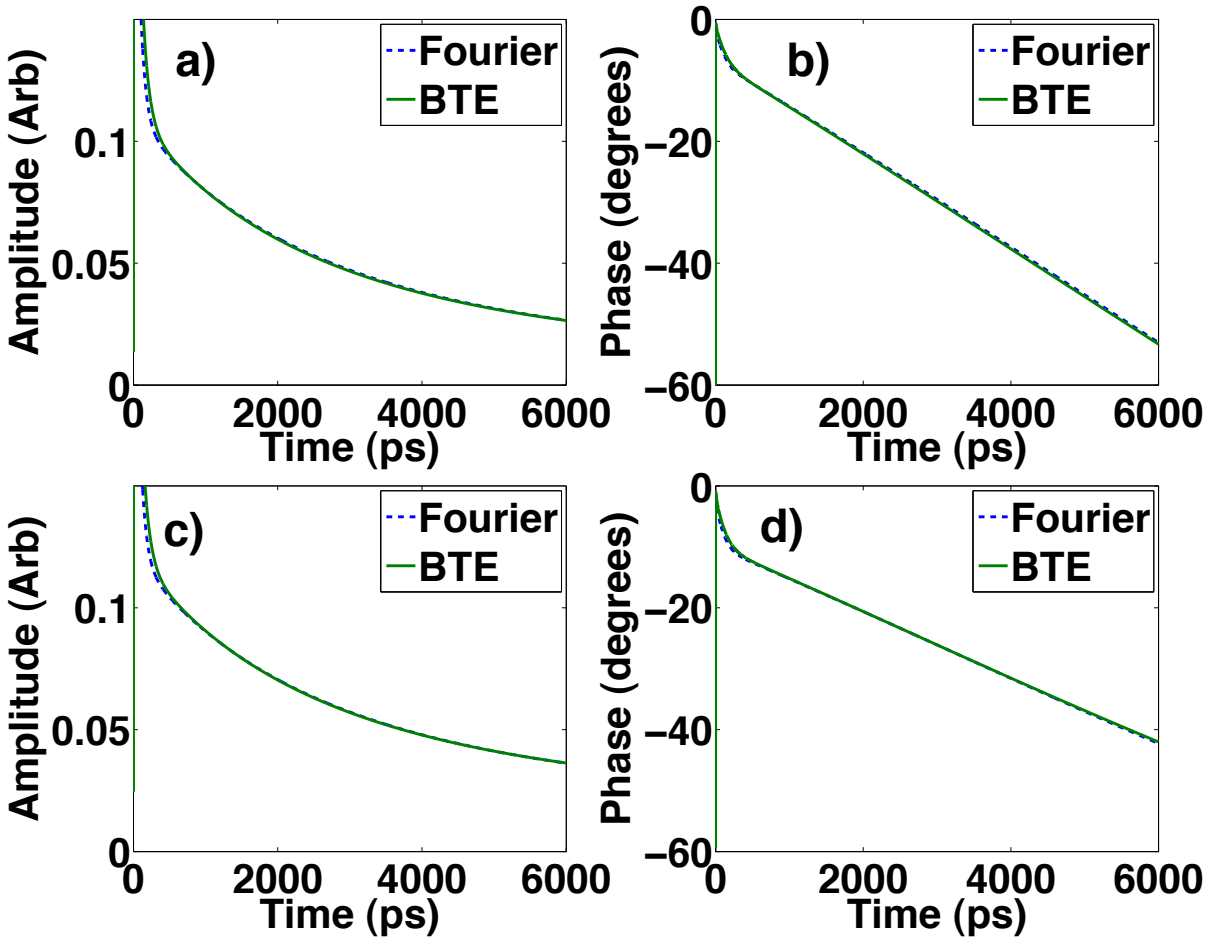

FIG. 5: Typical multi-pulse responses at different modulation frequencies calculated from the single-pulse response for the BTE and Fourier's law at T=300 K. (a) Amplitude and (b) phase responses at a modulation frequency of 15 MHz; (c) amplitude and (d) phase responses at a modulation frequency of 6 MHz. Both fits correspond to effective thermal conductivity k_{eff} = 100 W/mK and interface conductance $G = 1.0 \times 10^8$ W/m^{2}K and therefore do not not predict a modulation-frequency dependence of thermal conductivity.

dent thermal conductivity, then, the single-pulse response must deviate from the Fourier's law prediction such that the multi-pulse response corresponds to different thermal conductivities at different modulation frequencies. However, as can be seen in Fig. 4, the single-pulse BTE solution can be fit using a Fourier's law response with an effective thermal conductivity. Because the BTE response and Fourier's law response with effective properties are essentially identical, the multi-pulse response of the BTE must yield a thermal conductivity equal to its original effective value regardless of the modulation frequency. Thus, the present BTE calculation does not predict a modulation-frequency dependent thermal conductivity.

This lack of frequency dependence is demonstrated in Fig. 5. Here, we have used Eq. 23 to calculate the multi-pulse response of the BTE solution and the Fourier's law solution with the effective properties k_{eff}=100 W/mK and $G = 1.0 \times 10^8$ W/m^{2}K. As the figure shows, this same set of effective parameters can explain both the amplitude and phase responses of the BTE at two different modulation frequencies, 6 and 15 MHz. We have calculated the multi-pulse responses at several different frequencies in the MHz range and obtained the same result. Calculating the multi-pulse response at lower modulation frequencies is difficult because up to 1 μs of the BTE solution must be computed, but based on the above discussion we do not expect to observe a frequency dependence even at these lower frequencies.

It is interesting to note that experimentally, a modulation frequency effect has not been observed in pure silicon. In our recent work, we measured the thermal properties of silicon at cryogenic temperatures and found only a laser beam dependence of the thermal conductivity.[13] Koh and Cahill observed the modulation frequency effect only for

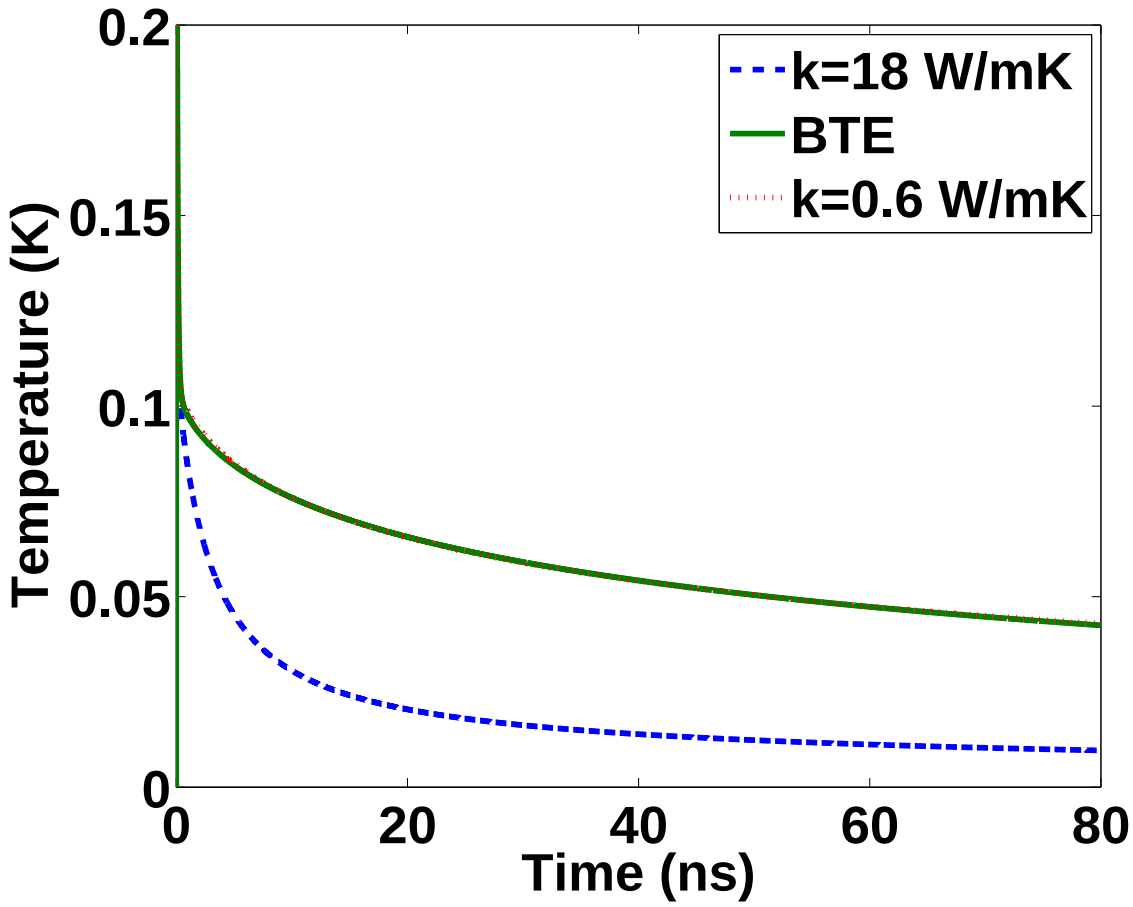

FIG. 6: Surface temperature (relative to a reference temperature of 300 K) versus time for silicon with a dilute point defect scattering rate predicted by the BTE (solid line), along with the solutions from Fourier's law for k=18 W/mK (dashed line) and k=0.6 W/mK (dotted line) at T = 300 K. The BTE solution almost exactly matches the curve with a reduced effective thermal conductivity of 0.6 W/mK, indicating that there is no modulation frequency dependence of the thermal conductivity.

semiconductor alloys. To determine whether the model predicts a modulation frequency dependence for alloys, we performed the same computation except with the point defect scattering rate increased by a factor of 10^3. This scattering rate corresponds to a material with a dilute point defect concentration. If a modulation frequency effect is present in the alloy case, the BTE temperature decay curve should deviate from a Fourier's law response. However, Fig. 6 shows that the BTE curve can again be fit by Fourier's law, although with a drastically different thermal conductivity, $k = 0.6$ W/mK, and interface conductance, $G = 0.3 \times 10^8$ W/m^{2}K, from the input values of $k = 18$ W/mK and 1.1×10^8 W/m^{2}K, respectively. The discrepancy is larger than in the pure silicon case, Fig. 4(a), because the strong scattering of high frequency modes leaves a larger fraction of heat carried by low frequency, long MFP modes. The calculation still does not predict a modulation frequency dependence of the thermal conductivity. The discrepancy between the calculation and experiment is puzzling and is an interesting topic for further study.

VI. CONCLUSION

In this paper, we have numerically solved the transient, one-dimensional, frequency-dependent BTE, including polarization, in order to better understand how phonon MFPs can be extracted from measurements of quasiballistic heat transfer. We solved the equation for a double layer structure of a metal film on a substrate to facilitate comparison with transient thermoreflectance experiments. Our results indicate that phonons with MFPs longer than the thermal penetration depth do not contribute to the measured thermal conductivity, providing a means to probe the MFP

distribution. The simulation also predicts that quasiballistic effects should be apparent even at room temperature in silicon or semiconductor alloys, and did not predict a modulation frequency dependence of thermal properties, contrary to experimental observations. These discrepancies offer opportunities for future investigation.

Acknowledgements

The authors would like to thank David Cahill for useful discussions. This material is partially based upon work supported as part of the "Solid State Solar-Thermal Energy Conversion Center (S3TEC)," an Energy Frontier Research Center funded by the U.S. Department of Energy, Office of Science, Office of Basic Energy Sciences under Award Number: DE-SC0001299/DE-FG02-09ER46577 (G.C.), by the Center for Clean Water and Clean Energy at MIT and KFUPM (A.M., S.M., B.S.Y.), and by the NSF to A.M.

* Electronic address: gchen2@mit.edu

[1] H. Casimir, Physica **5**, 495 (1938).
[2] A. Majumdar, Journal of Heat Transfer **115**, 7 (1993).
[3] G. Chen, Physical Review B **57**, 14958 (1998).
[4] D. G. Cahill, W. K. Ford, K. E. Goodson, G. D. Mahan, A. Majumdar, H. J. Maris, R. Merlin, and S. R. Phillpot, Journal of Applied Physics **93**, 793 (2003).
[5] R. Chen, A. I. Hochbaum, P. Murphy, J. Moore, P. Yang, and A. Majumdar, Phys. Rev. Lett. **101**, 105501 (2008).
[6] G. Chen and C. L. Tien, Journal of Heat Transfer **114**, 636 (1992).
[7] R. J. von Gutfeld and A. H. Nethercot, Phys. Rev. Lett. **12**, 641 (1964).
[8] M. Highland, B. C. Gundrum, Y. K. Koh, R. S. Averback, D. G. Cahill, V. C. Elarde, J. J. Coleman, D. A. Walko, and E. C. Landahl, Phys. Rev. B **76**, 075337 (2007).
[9] G. D. Mahan and F. Claro, Phys. Rev. B **38**, 1963 (1988).
[10] G. Chen, Journal of Heat Transfer **118**, 539 (1996).
[11] M. E. Siemens, Q. Li, R. Yang, K. A. Nelson, E. H. Anderson, M. M. Murnane, and H. C. Kapteyn, Nature Materials **9**, 26 (2009).
[12] Y. K. Koh and D. G. Cahill, Physical Review B (Condensed Matter and Materials Physics) **76**, 075207 (2007).
[13] A. J. Minnich, , J. A. Johnson, A. J. Schmidt, K. Esfarjani, M. S. Dresselhaus, K. A. Nelson, and G. Chen, Physical Review Letters **107**, 095901 (2011).
[14] A. J. Minnich and G. Chen, (in preparation) (2011).
[15] Y. K. Koh, Ph.D. thesis, University of Illinois, Urbana Champaign (2010).
[16] A. A. Joshi and A. Majumdar, Journal of Applied Physics **74**, 31 (1993).
[17] S. Sinha and K. Goodson, Microelectronics Journal **37**, 1148 (2006).
[18] Q. Hao, G. Chen, and M.-S. Jeng, Journal of Applied Physics **106**, 114321 (2009).
[19] N. G. Hadjiconstantinou, G. A. Radtke, and L. L. Baker, Journal of Heat Transfer **132**, 112401 (2010).
[20] S. V. J. Narumanchi, J. Y. Murthy, and C. H. Amon, Journal of Heat Transfer **126**, 946 (2004).
[21] A. Ward and D. A. Broido, Phys. Rev. B **81**, 085205 (2010).
[22] A. Majumdar and P. Reddy, Applied Physics Letters **84**, 4768 (2004).
[23] P. G. Klemens, Phys. Rev. **148**, 845 (1966).
[24] G. Chen, *Nanoscale Energy Transport and Conversion* (Oxford University Press, New York, 2005).
[25] *http://www.ioffe.rssi.ru/sva/nsm/semicond/index.html. accessed april 2008.*
[26] P. K. Schelling, S. R. Phillpot, and P. Keblinski, **80**, 2484 (2002), ISSN 00036951, URL http://dx.doi.org/10.1063/1.1465106.
[27] E. S. Landry and A. J. H. McGaughey, Phys. Rev. B **80**, 165304 (2009), URL http://link.aps.org/doi/10.1103/PhysRevB.80.165304.
[28] E. T. Swartz and R. O. Pohl, Rev. Mod. Phys. **61**, 605 (1989).
[29] A. S. Henry and G. Chen, Journal of Computational and Theoretical Nanoscience **5**, 141 (2008).
[30] M. G. Holland, Phys. Rev. **132**, 2461 (1963).
[31] *http://refractiveindex.info/?group=metals&material=aluminium. accessed september 2010.*
[32] A. J. Schmidt, X. Chen, and G. Chen, Review of Scientific Instruments **79**, 114902 (2008).